# Determination of principal characteristics of turbulent swirling flow along annuli

## Part 1: Measurement of time mean parameters

**B. R. Clayton and Y. S. M. Morsi***

Turbulent swirling flows along the annulus formed between two concentric stationary cylinders have been studied. Hot-wire anemometry was used to detect radial variations of velocity components and the data presented in Part 1 of the investigation describes time mean measurements. Pressure measurements along the length of the outer, concave, cylindrical surface were obtained from wall tappings attached to a pressure transducer. Flow visualization using tufts indicated general swirl decay phenomena and these have been confirmed by the traverse data. The swirl flow rig was designed to incorporate suction systems to remove boundary layers from all walls preceding the test section. In this way the essentially free vortex generated by a circumferentially disposed set of guide vanes in the inlet bellmouth of the apparatus could be efficiently transferred to the test section entry region. This feature has not been incorporated by other workers and so their reported results depend on the upstream boundary layer flow, making correlation of data difficult. The data shown in this paper indicate the complex nature of swirling flow development in an annulus although it is not yet possible to be precise about the initial phases

**Keywords:** *turbulence, swirl, annuli, concentric tubes, swirl decay*

Swirling flows are usually considered to be those for which the tangential component of velocity makes a significant contribution to the resultant. This paper is concerned principally with swirling flow passing along the annulus formed by two co-axial pipes of different diameter but equal length and with one wholly inside the other. The addition of swirl to an initially axisymmetric throughflow introduces a number of favourable characteristics, such as an increase in path length (although at the expense of increased energy dissipation by friction), a decrease in flow area and the introduction of an angular acceleration to fluid particles. There are a number of engineering applications which may benefit from swirling flows; for example:

- The rate of heat transfer in heat exchangers can be increased by introducing swirl without paying the penalty of excessive eddy losses associated with wakes shed by transverse tubes and fins.
- Improvements in the design and performance prediction of various types of turbomachinery can be developed on the basis of a better understanding of swirling flow in blade passages.
- Similar remarks apply to the development of vortex separators, nozzles for rocket propulsion, fluidic devices and so on.

Despite the importance of these applications, a thorough understanding of turbulent swirling flows has still to be achieved even though several significant studies have been reported in the literature. Some of these studies are related to swirling flows in pipes, the results from which have relevance to annular flows.

King *et al*[1] examined experimentally the phenomenon of reverse motion in the axial direction of strongly swirling, constant density flow through a fixed pipe. The swirl was induced by the injection of fluid through the symmetric tangential inlet ports perpendicular to the pipe. From the measurements of pressure and velocity it was concluded that the flow could be roughly divided into free and forced vortex regions. With increasing axial distance from entry, the initial forced vortex was found to decay into a free vortex. A region of reverse axial flow was detected in the core region of the pipe and the radius of this region was found to decrease to zero with increasing axial distance. No such behaviour has been reported for annular flows and no reversal was found for the flows investigated by the present authors.

Wolf *et al*[2] studied the decay of turbulent swirling flow along a stationary pipe and measured an increase in the decay of swirl with increasing initial swirl and decreasing Reynolds number. Backshall[3] concentrated on the characteristics of turbulent boundary layers for swirling flow in a pipe. He subsequently suggested that the resultant of the time mean axial and tangential velocities is well approximated by the logarithmic law. This behaviour does, of course, help considerably in the formulation of theoretical analyses.

Surface roughness was included as a variable in the experiments by Senoo and Negata[4]. The data were used to estimate shear stress and wall pressure at locations along

* Department of Mechanical Engineering, University College London, Gower Street, London WC1E 6BT, UK
Received 29 March 1984 and accepted for publication on 22 August 1984

a pipe. The change in axial velocity resulting from swirl along pipes was investigated by Yajnik and Subbaiah[5]. They found that the measured axial velocity profiles obeyed the law of the wall applicable to turbulent parallel flow. Furthermore, a logarithmic skin friction law was deduced which contained only one additional component that depended on the strength of the initial swirl velocity. A simple investigation by Murakami and Osami[6] was used to obtain the longitudinal shear stress and pressure at the wall of a pipe.

There have been relatively few detailed experiments on turbulent swirling flows along annuli formed by co-axial smooth pipes and that of Yeh[7] was one of the first. He attempted to develop a semi-empirical model to predict the thickness and other characteristics of the boundary layers on both the inner (convex) and outer (concave) walls for both swirling and non-swirling flows. In addition, some measurements of turbulence intensity were undertaken.

Brighton and Jones[8] examined radial variations of axial velocity for turbulent flows along an annulus at locations where the flow was considered to be fully developed, ie at distances from the annulus inlet where the velocity profile was invariant with axial distance. Different radius ratios and Reynolds numbers were used but swirl was not considered. The authors found that a log law could be used for the velocity variation close to the outer wall but some disparity existed near the inner wall. Another study of the development of turbulent boundary layers for non-swirling annulus flows was published by Okiishi and Serovy[9] who gave particular attention to the effects of square-edged and rounded entrance ducts on the flow behaviour along the annulus.

Quarmby[10] pointed out some inconsistencies in earlier work regarding the radial location of maximum velocity and the values of wall shear stresses which resulted in uncertainties about the similarity law of the wall in annular turbulent flow. The location of maximum velocity was found to be different for laminar and turbulent flows and depended on Reynolds number and radius ratio. Furthermore he could not fit his data to a universal law of the wall except for the outer profile at large Reynolds number and radius ratios.

Gutstein *et al*[11] used a helical vane of constant pitch and a circular tube centre body inserted in a larger pipe to generate a swirling annulus flow. They concentrated on measurements of pressure drop along the annulus and then considered the drop consisted of two components related to momentum loss and friction loss. In their analysis they assumed a uniform axial velocity and linearly varying tangential velocity across the annulus, both of which are quite unrealistic.

Scott and Rask[12] conducted a careful and extensive study of the development of the axial velocity profile and the decay of tangential velocity profile along an annulus. The main thrust of the work was directed towards a data reduction technique for obtaining shear stresses and eddy diffusivity across the annulus by numerical integration of the momentum equations. Owing to the lack of relevant data on turbulence measurements, the authors neglected all turbulence intensities that appeared in the integral form of the momentum equations.

This paper adds further comprehensive information on the actual development and decay of the swirling flow characteristics along a constant section annulus for different inlet swirl intensities, Reynolds numbers and radius ratios. The data presented describe time mean properties of the flow and in Part 2 a discussion is given of turbulence parameters[13].

## Experimental techniques

Fig 1 is a schematic layout of the swirling flow rig used for the experiments. The apparatus is centred about an overall conditioning section which was designed to carry out three functions:

## Notation

| | |
|---|---|
| $A$ | Cross-sectional area of annulus, $\pi(r_0^2-r_i^2)$ |
| $C_p$ | Pressure coefficient, $p/\frac{1}{2}\rho U_{av}^2$ |
| $C_{p_o}$ | Pressure coefficient on surface of outer (concave) tube, $p_0/\frac{1}{2}\rho U_{av}^2$ |
| $D_h$ | Hydraulic diameter, $d_0-d_i$ |
| $d_i$ | Diameter of inner (convex) tube surface |
| $d_0$ | Diameter of outer (concave) tube surface |
| $n$ | Number of turns |
| $p$ | Gauge pressure |
| $p_0$ | Gauge pressure on outer (convex) tube surface |
| $Q$ | Volume flow rate |
| $R$ | $r/r_0$ |
| $Re$ | Reynolds number, $Qr_0/Av$ |
| $r$ | Radius |
| $r_i$ | Radius of inner (convex) tube surface |
| $r_0$ | Radius of outer (concave) tube surface |
| $S_i$ | Swirl intensity |
| $\hat{S}_i$ | Swirl intensity at inlet to working section |
| $U$ | $\bar{U}/U_{av}$ |
| $U_{av}$ | $Q/A$ |
| $U_{max}$ | Maximum value of $U$ |
| $\tilde{U}$ | $\bar{U}+u'$ |
| $\bar{U}$ | Time mean axial velocity |
| $u$ | $u'/U_{av}$ |
| $u'$ | Fluctuating axial velocity |
| $V$ | $\bar{V}/U_{av}$ |
| $\tilde{V}$ | $\bar{V}+v'$ |
| $\bar{V}$ | Time mean radial velocity |
| $v$ | $v'/V_{av}$ |
| $v'$ | Fluctuating radial velocity |
| $W$ | $\bar{W}/U_{av}$ |
| $W_{max}$ | Maximum value of $W$ |
| $\tilde{W}$ | $\bar{W}+w'$ |
| $\bar{W}$ | Time mean tangential velocity |
| $w$ | $w'/U_{av}$ |
| $w'$ | Fluctuating tangential velocity |
| $x$ | Axial distance measured from entry to working section |
| $\alpha$ | Radius ratio, $r_i/r_0$ |
| $\beta$ | Flow angle, arctan $(W/U)$ |
| $\gamma$ | $(r-r_i)/(r_0-r_i)$ |
| $\nu$ | Kinematic viscosity of fluid |
| $\rho$ | Density of fluid |
| $\Psi$ | Guide vane setting angle |

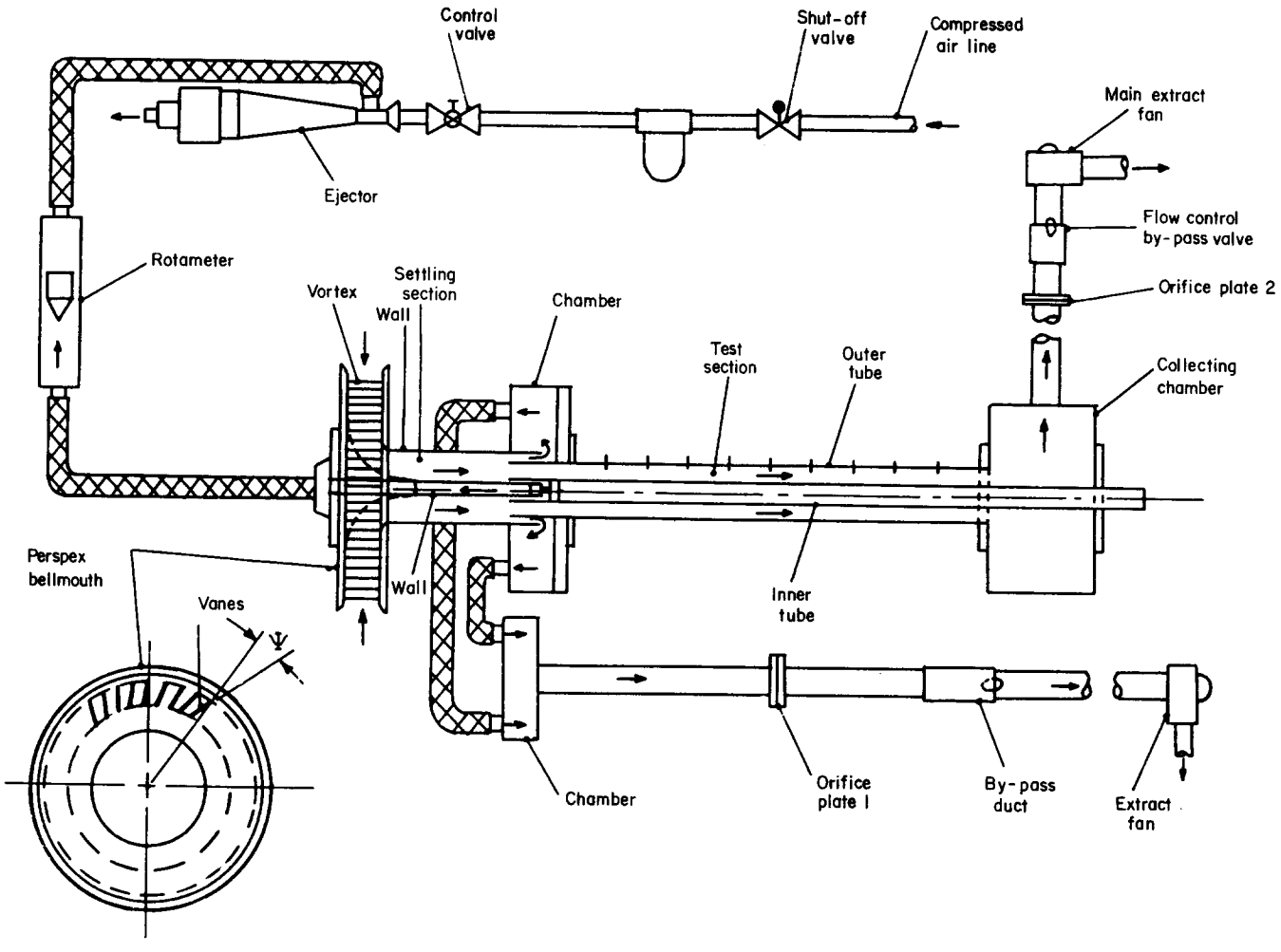


*Fig 1 Annular swirling flow rig layout*

- to generate a vortex of the desired characteristics, generally of a free vortex nature;
- to transfer the vortex to a swirling flow progressing along an annulus;
- to remove the shear flow adjacent to the annular walls before entry to the test section annulus.

It was decided at the outset to remove all flow near to walls between the inlet to the rig and inlet to the working section so that details of the flow development along an annulus could be studied following the entry of a potential flow to the working section. No previous work on annulus flows has included techniques for doing this and so the shear flows in the working section, which are governed by the flows approaching the entry to it, could not be correlated in a general manner, or even within the individual tests themselves.

The vortex was generated by a set of forty guide vanes (Fig 1) machined from aluminium alloy and placed symmetrically round the entrance to the Perspex bellmouth. These guide vanes have several advantages over other vortex generators. For example, unlike twisted tape or coiled wire, the guide vanes do not generate significant secondary flows. Furthermore, considerable flexibility in the geometry of the swirl flow profile generated can be obtained either by reducing the number of vanes or departing from symmetry. In general, nearly free-vortex flow was used in these experiments. The swirl angle was set by adjusting the angular orientation $\Psi$ of each value to a specified value between 0 and 90° relative to the radial direction using a specially designed jig. The function of the bellmouth was to transport the vortex flow into a settling section with as little disturbance as possible so that a progressive swirling flow was developed before passing on to the test section. The settling section consisted of two concentric circular section tubes fixed at one end to the bellmouth. Although the length of this section was limited to 150 mm, a boundary layer of significant thickness built up on the walls and within the bellmouth owing to the helical path traced out by the flow. It was necessary, therefore, to remove these wall shear flows if a potential flow at entry to the test section were to be achieved. Two independent suction systems were installed to draw off flow from each wall of the settling section.

Rather than incorporate porous walls surrounding the settling section, the walls were impermeable and the shear flow subsequently collected in chambers adjacent to the test section entry region. The inner wall suction was adjusted by a shut-off valve and a control valve attached to a compressed air line so that a vacuum was created on the ejector. A rotameter measured the flow rate of air drawn off by the ejector. The inner tube of the settling section had a smaller diameter than the inner tube of the test section into which it is plugged. To ensure uniformity and stability of the flow entering the test section, the inner suction air was extracted through twelve

**Table 1 Location of traverse stations in working section**

*A: Radius ratio* $\alpha$=0.51

| Station | 1 | 2 | 3 | 4 | 5 | 6 | 7 | 8 | 9 | 10 |
|---|---|---|---|---|---|---|---|---|---|---|
| Axial distance from entry $x$, mm | 0 | 92.0 | 179.0 | 272.2 | 359.3 | 451.9 | 539.0 | 631.6 | 718.7 | 811.3 |
| $x/r_o$ | 0 | 1.69 | 3.28 | 4.99 | 6.59 | 8.29 | 9.89 | 11.59 | 13.19 | 14.89 |
| $x/D_h$ | 0 | 1.74 | 3.38 | 5.14 | 6.78 | 8.53 | 10.17 | 11.92 | 13.56 | 15.31 |

*B: Radius ratio* $\alpha$=0.61

| Station | 1 | 2 | 3 | 4 | 5 | 6 | 7 | 8 | 9 | 10 | 11 | 12 |
|---|---|---|---|---|---|---|---|---|---|---|---|---|
| Axial distance from $x$, mm | 0 | 69.0 | 127.0 | 185.0 | 243.0 | 301.0 | 359.0 | 417.0 | 532.0 | 647.0 | 762.0 | 877.0 |
| $x/r_o$ | 0 | 1.51 | 2.76 | 4.04 | 5.31 | 6.58 | 7.85 | 9.11 | 11.63 | 14.14 | 16.66 | 19.17 |
| $x/D_h$ | 0 | 1.94 | 3.58 | 5.21 | 6.85 | 8.48 | 10.11 | 11.75 | 14.99 | 18.23 | 21.46 | 24.70 |

equi-spaced orifices. Air near the outer walls of the settling section was drawn through eight orifices symmetrically spaced about the entry region of the outer tube of the test section. After collection in the chambers, the suction air passed through orifice plate 1 to determine the flow rate, a control device in the form of an adjustable by-pass duct and thence to an extract fan.

The chamber at entry to the test section was constructed to allow tubes of different diameter to be fitted to give different annulus areas and radius ratios. The inner tube was of constant outer diameter, 56 mm, and made of brass to aid flow visualization. This tube occupied the length of the test section and passed through the collecting chamber in order to reduce shock losses at exit from the test section. The leading edges of both tubes making up the test section were carefully streamlined and the centre lines of each were precisely aligned. The outer tube was constructed of Perspex and carried a series of tapping holes used for pressure measurements and, suitably modified, for velocity traverses with a hot-wire anemometer. Two outer tubes were used of diameter 109 mm and 91.5 mm which gave inner-to-outer radius ratios of 0.51 and 0.61 respectively. The complete test section, of length 938 mm, was supported by a rigid framework capable of maintaining the concentricity of the tubes. Air from the collecting chamber passed through orifice plate 2 to determine the flow rate of air along the annulus, and thence through a flow control by-pass valve to the main extract fan.

A traversing mechanism was designed to carry hot-wire anemometer probes across the two annuli used, ie traverse distances of 26.5 mm and 17.8 mm. Angular and linear displacements were measured with the aid of transducers. A series of radial holes were made in the wall of the outer tube to provide access for the traversing instruments and thus to locate the traversing stations shown in Table 1. Precision made inserts were fitted into the holes in order to support the probe body and the inner surface of each insert was machined with high accuracy to the correct curvature of the inner (concave) surface of the outer tube. On the diametrically opposite side of the outer tube a series of pressure tapping holes were drilled to correspond with the longitudinal positions of the traverse stations. Further details of the apparatus and estimates of experimental accuracy are given by Morsi[14].

## Flow visualization

Several flow visualization techniques were considered for providing a general illustration of the flow. The use of smoke was abandoned owing to its rapid diffusion in turbulent flow. As some forty minutes were required for steady mean values to prevail in the swirling flow rig, to eliminate moisture from the compressed air supply and ensure a constant air temperature, the use of oil flow techniques at the tube surfaces was rejected. Even if the oil could have been applied to the surfaces of the working section, which would have been difficult, evaporation would have taken place long before sensible flow patterns could have been traced.

As a result of these considerations tufts were used to indicate the flow characteristics, in particular swirl angle and decay along the annulus at different radial positions. A dramatic picture of these events may be seen in Fig 2 which shows typical paths taken up by a long continuous thread anchored in the settling section and following a streamline close to the inner wall of the test section. Further sets of tufts were attached by universal links to thin radial wires located at the traverse stations to give an indication of the radial variations of swirl angle.

The success of the inner and outer wall suction devices in terms of balanced flow can be judged by the lack of any indication of separation in the entrance region of the test section. It was also observed that if the correct amounts of suction were not applied, then separation regions appeared near to the leading edges of the inner and outer test section tubes. The absence of large scale disturbances once tests were well underway suggested that no unsteady effects from the main extract fan were propagated into the annulus. Assuming that gravitational forces on the threads are negligible compared with aerodynamic forces suggests that the thread follows a mean streamline and thus indicates swirl decay. Fig 2 shows that the angle $\beta$ of the tangent line to this thread

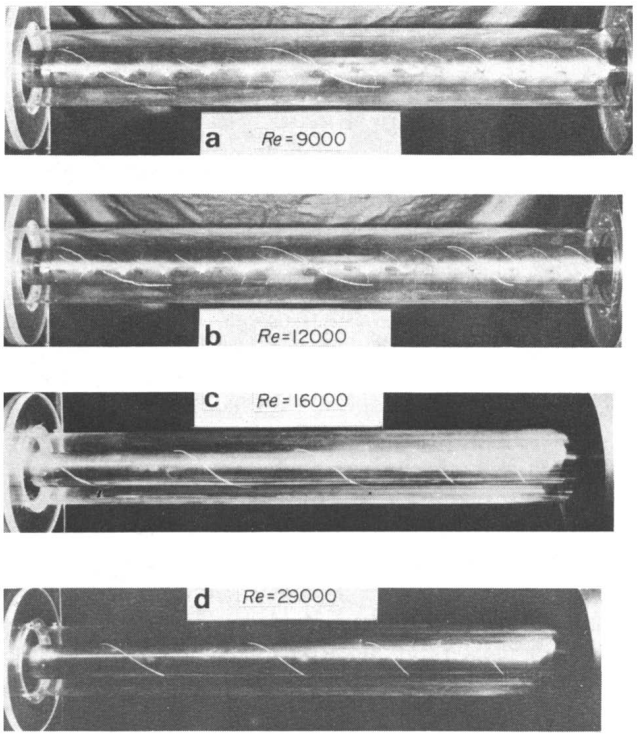


*Fig 2 Visualization of tuft in swirling annular flow for $\alpha=0.51$ and $\Psi=45°$. Flow from right to left*

and to the radially located tufts, measured relative to the axial direction, decreases progressively with increasing axial distance downstream. In Fig 2(b), for example, $\beta$ decreases from an inlet value of 45° to 21° near the outlet so that the pitch length of the swirl increases substantially. This pitch length increases more rapidly with downstream distance as the inner wall is approached, implying a more rapid axial decrease of shear stress there than at the outer wall, supporting the conclusion drawn by Yeh[7]. A careful scrutiny of all the patterns obtained showed that over the range of Reynolds number used, 9000–29000, the length of streamlines decreased with increasing *Re*.

The preceding points are seen more clearly in Fig 3 where the streamlines, represented by the length of thread, have been straightened out to give an indication of the current length of a particle path as a function of axial distance along the annulus for several values of *Re* and $\Psi$.

## Experimental results

In this and the following section a comprehensive set of data are shown which describe the development of an initially potential swirling flow along the annulus formed by two sets of co-axial tubes of radius ratios $r_i/r_0=\alpha=0.51$ and 0.61. Where possible, comparisons are made with previous work although it must be admitted that other published sources of coherent data are rather scarce. Hot-wire traverses, using the novel measurement techniques for single wires described elsewhere[15], have been analysed to provide radial variations of all three mean velocity components at the axial stations shown in Table 1. Wall pressure measurements were also obtained at corresponding locations. Morsi[14] gives a full presentation and discussion of the large number of measurements taken. Estimations of accuracy indicate that, for the data presented in this paper, results are generally accurate to within $\pm 2\%$.

Instantaneous local velocity components may be represented by the sum of a mean and a fluctuating velocity, ie:

$$\tilde{U}=\bar{U}+u' \qquad \tilde{V}=\bar{V}+v' \qquad \tilde{W}=\bar{W}+w' \qquad (1)$$

The average velocity of the constant density flow passing along the annulus is given by the volume flow rate divided by the cross-sectional area:

$$U_{av}=\frac{Q}{A}=\frac{Q}{\pi(r_0^2+r_i^2)}$$

where $Q$ was deduced from the pressure differential over orifice plate 2 in Fig 1 and frequently checked against the results of integrating the axial velocity variation at entry to the test section. Velocity profiles can then be constructed with respect to dimensionless parameters on dividing instantaneous velocities by $U_{av}$:

$$\frac{\tilde{U}}{U_{av}}=U+u \qquad \frac{\tilde{V}}{U_{av}}=V+v \qquad \frac{\tilde{W}}{U_{av}}=W+w \qquad (2)$$

where $U=\bar{U}/U_{av}$ and $u=u'/U_{av}$ etc. Scales for radial coordinates are alternatively given as $r/r_0=R$ and $(r-r_i)/(r_0-r_i)=(R-\alpha)/(1-\alpha)=\gamma$. Most of the data were collected for $\alpha=0.51$ at $Re=28\,700$ and 22 400 and our concern here is with variations of $U$, $V$ and $W$.

### Axial velocity profiles

Radial distributions of the axial velocity component along the annulus are shown in Fig 4 in terms of the preceding dimensionless variables for $\alpha=0.51$ and $Re=28\,700$. The locations of the traverse stations correspond to arrangement A in Table 1. For the bellmouth guide vanes set radially, ie $\Psi=0$ and no swirl, the axial velocity at inlet to the test section is a sensibly uniform potential flow, but then alters radically with distance along the axis. For the sake of clarity the origin of each profile is displaced consecutively to the left by an increment of 0.15 in the $U$ scale. There is a tendency for higher axial velocities to be located near the inner wall and for central portions of constant velocity to diminish with

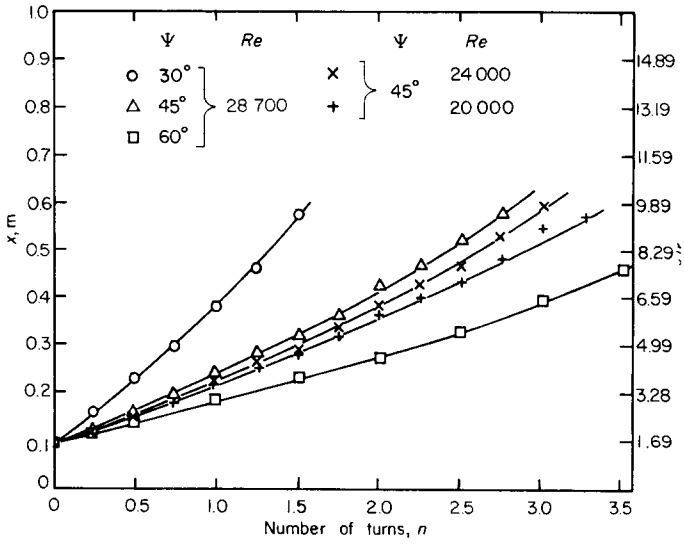


*Fig 3 Relative length of particle paths indicated by number of circumferential circuits completed*

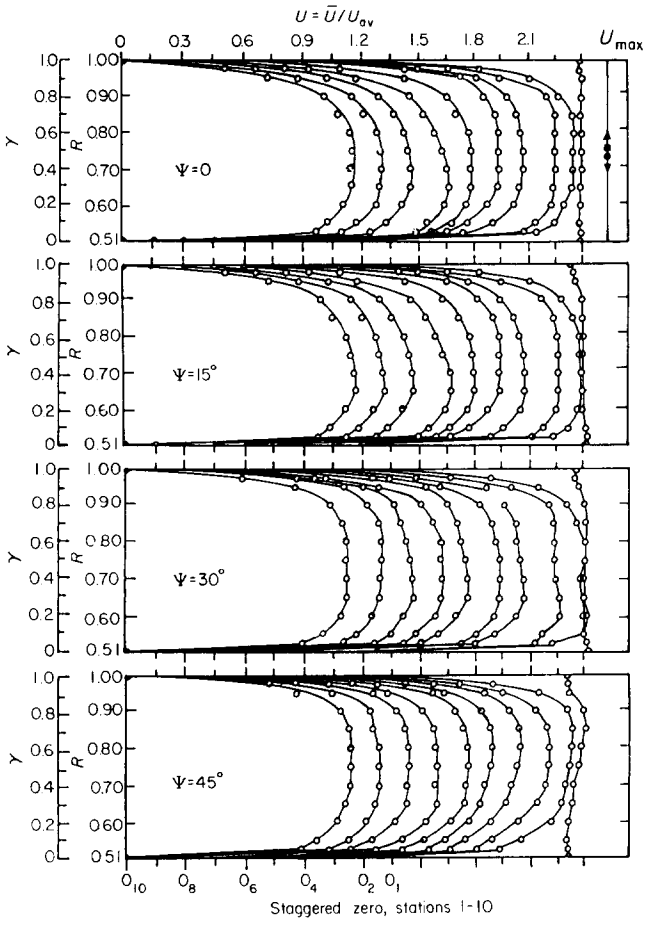


*Fig 4 Variation of axial velocity component for $\alpha=0.51$ and* Re $=28\,700$. *Also shown are radial locations of* $U_{max}$ *in fully developed flow:* ▼ *Scott and Rask*[12] *for $\alpha=0.4$, $\Psi=45°$;* ● *Present for $\alpha=0.51$, $\Psi=0°$ and 45°;* ■ *Brighton and Jones*[8] *for $\alpha=0.56$, $\Psi=0°$;* ▲ *Present for $\alpha=0.61$, $\Psi=45°$ and 60°*

increasing $x$ (Table 1). The slight dip in the profile close to the outer wall at inlet cannot be explained easily, but may be the result of some small imperfection in the rig since the characteristic remained throughout a reasonable range of suction adjustments.

For other values of $\Psi$ it is seen that $U$ at entry is scarcely changed; indeed throughout the annulus the magnitude of $U$ is little affected by changes of $\Psi$ except in the early developing region represented by $x$ up to station 5. It may be seen that as the swirl (and $\Psi$) increases, the maximum of corresponding $U$ profiles moves away from the inner wall and for $\Psi=45°$ is nearer to the outer wall for stations 1 to 5 between which rapid development of the flow takes place. This behaviour results from the increasing effect of higher tangential shear stresses on the outer compared with the inner wall. The effect of reducing $Re$ from 30 000 to 20 000 was found to be an increase in $U$ at a given $r$ of about 3.5% on average.

Also shown in Fig 4 is the radial location of maximum $U$ for several $\alpha$ and $\Psi$ from both the present work and those of other workers. Although, where possible, comparable Reynolds numbers were chosen, these were not all the same; however, it has been shown here and elsewhere that the effects of $Re$ are modest. These data were taken from profiles in the fully developed region and it is seen that for a given $\alpha$, $U_{max}$ occurs at the same $R$ for widely ranging $\Psi$. Furthermore, $U_{max}$ moves nearer to the outer wall as $\alpha$ increases from 0.4 to 0.61.

## Tangential velocity profiles

A set of tangential velocity profiles for $W$ as a function of radial and axial location is shown in Fig 5 for $\alpha=0.51$, $\Psi=15°$, 30° and 45° and $Re=28\,700$. A number of important features may be observed. At the inlet to the test section the tangential velocity decreases almost linearly with increasing radial distance from the inner wall. Thus, although the symmetrically displaced and equally deflected guide vanes in the bellmouth would be expected to generate a free vortex for inviscid flow, in reality by the time the flow has reached the test section, the complex interchanges taking place between the axial and tangential energy and momentum components over the flow passage distort the swirl distributions to those depicted in Fig 5. For all cases the maximum value, $W_{max}$ remains quite close to the inner wall and migrates slowly outwards with increasing distance downstream. There is a tendency for each radial variation to depict a forced vortex behaviour towards the inner wall, a free vortex behaviour in the core region and an approximately linear reduction as the outer wall is approached. At a given radius $W$ decays with distance downstream, rapidly in the developing region but although the rate decreases along the annulus we must expect swirl to be eventually eliminated well downstream, essentially at infinity in a mathematical model.

Another feature that is consistent throughout is the greater extent of the boundary layer on the outer (concave) wall compared with that on the inner wall, as shown also by the $U$ profiles (including the case $\Psi=0$). Shear stresses must therefore be greater on the outer than the inner surface and this point receives further support on analysis of the turbulence components reported elsewhere[13].

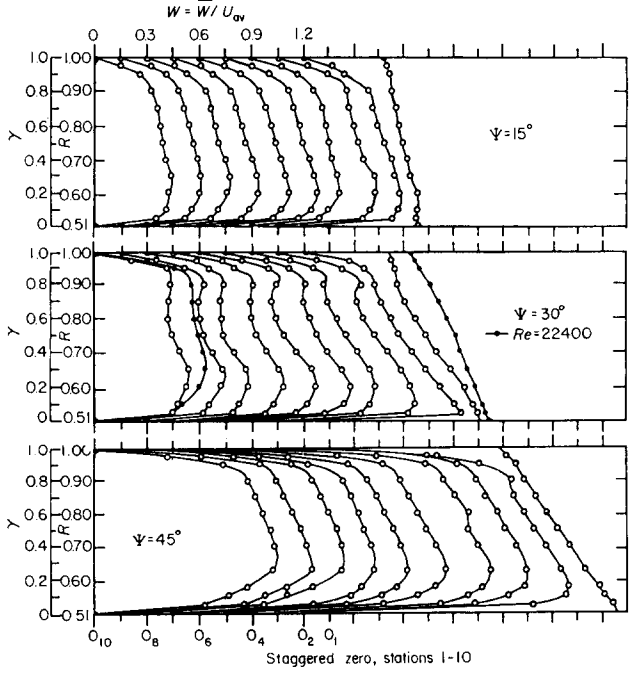


*Fig 5 Variation of tangential velocity component for $\alpha=0.51$ and* Re $=28\,700$

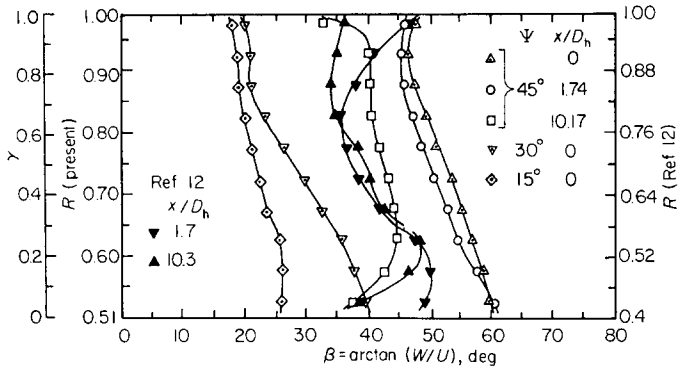


*Fig 6 Variation of flow angle for $\alpha = 0.51$ and Re ~ 28 700. Results from Scott and Rask[12] for $\alpha = 0.4$ and Re ~ 13 × 10⁴ are included*

Fig 5 (middle) shows the entrance and final profiles for $Re = 22\,400$. At the entry $W$ is very nearly linear and $\partial W/\partial r$ significantly less than at the higher $Re$. At traverse station 10 the $W$ profile has a similar shape at both $Re$ but has decayed less for the lower $Re$, consistent with higher entry values. Integration across the annulus to determine the entry angular momentum of the flow, in dimensionless form, produced a value for $Re = 22\,400$ some 30% higher than that for $Re = 28\,700$. A similar result for changes in $Re$ has been reported by Wolf *et al*[2] for swirling flow in a pipe. The reason for this is that $Re$ varies linearly with velocity but the equilibrium between centrifugal forces and radial pressure gradient does not. Thus the radial variation of $U$ changes little with $Re$ (as one might expect, 'scale' effect is small at these Reynolds numbers) but we see much larger changes in $W$.

From the $U$ and $W$ profiles we can determine the radial variation of flow angle at a given traverse station since $\beta = \arctan(W/U)$. The results of these calculations for the entry profiles shown in Fig 5 are given in Fig 6 which serves as a correlation between $\beta$ and $\Psi$. Values of $\beta$ calculated from the velocity distributions cannot be used directly to provide $\beta$ near a wall and thus a check on the angles of the tuft indicated in Fig 2. To do this we must determine the ratio of tangential to axial shear forces, or stresses, at the inner surface since the tuft is aligned with the resultant force there. As an example, the angle calculated in this manner corresponding to the data of Fig 2(d) is 54° near the inlet compared with the tuft angle of 49°, a not unreasonable correlation in view of the uncertainties in the measurement of relevant parameters. Also included in Fig 6 are distributions of $\beta$ at corresponding values of $x/D_h$ and $\Psi = 45°$ for the present work ($\alpha = 0.51$ and $Re = 28\,700$) and that of Scott and Rask[12] where $\alpha = 0.4$ and $Re = 13 \times 10^4$. In both cases the inlet swirl distribution is nominally free vortex. It is difficult to see a clear-cut correlation here, but if one makes allowance for the effects of disparities in $Re$ on $W$ and recalls that no suction was applied by Scott and Rask[12] the data do not portray conflicting behaviour. Even so, it does highlight the considerable difficulty in bringing together experimental results of these complex flows from different sources in an effort to find common ground on which to generalize characteristics.

For internal flows, such as those considered here, radial velocities are likely to be small and so direct measurement would undoubtedly be inaccurate. The integration across the annulus of the longitudinal gradient of $rU$ was therefore used consistent with the continuity equation. Only at the entrance to the test section was $V$ found to vary significantly and even there $V$ was two orders of magnitude smaller than $U$. Thus $\beta$ could safely be used as an accurate descriptor of flow direction. Naturally, the variation of the resultant velocity $(U^2 + W^2)^{1/2}$ can be predicted from that of its components and shows a series of maxima nearer to the inner than the outer wall and a more rapid decay as $\Psi$ increases.

## Swirl intensity

Various expressions have been proposed[5] for the swirl intensity $S_i$. Here we shall consider $S_i$ to be the ratio of the total angular momentum flux to the total axial momentum flux, each evaluated over a given annulus cross-section, ie in dimensionless form:

$$S_i = \int_x^1 UWR^2 dR \Big/ \int_x^1 U^2 R dR \qquad (3)$$

Data were used from the $U$ and $W$ profiles previously discussed and Fig 7 shows the axial variation of $S_i$ as a proportion of the inlet (maximum) value $\hat{S}_i$ for different $\Psi$, $Re$ and $\alpha$. These curves suggest that the rate of decay of swirl increases with $\Psi$ and $\alpha$ but depends weakly on $Re$, other than in the entry region. There is also some support for these deductions from the previously discussed tuft observations. Furthermore, the analyses developed elsewhere[14,16] indicate the existence of distinct regions as swirling flow develops along an annulus from the inlet. However, complete confirmation of such behaviour requires more in the way of experimentation and a suitable programme of work to deal with this matter will commence shortly.

## Pressure variations

As explained earlier, pressure measurements from tappings linked to a transducer could only be made at the outer wall although values at the inner wall may be deduced from the radial pressure gradient variations. The dimensionless outer wall pressure, in the form of the

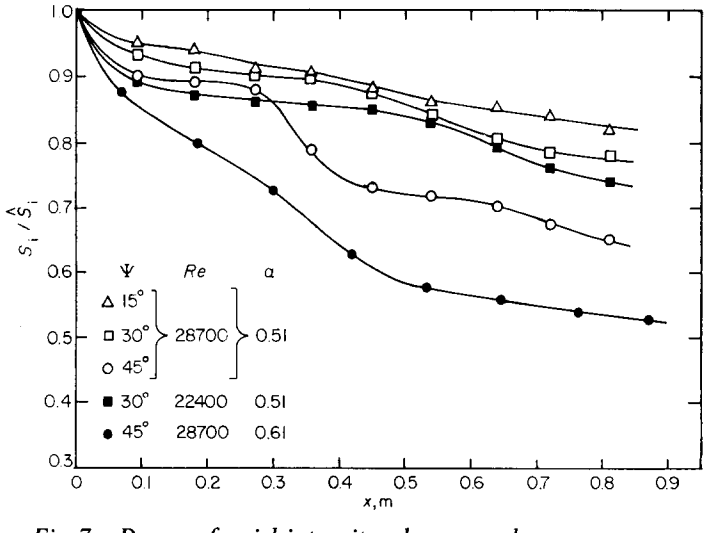


*Fig 7 Decay of swirl intensity along annulus.*

pressure coefficient:

$$C_{p_o} = p_0 / \tfrac{1}{2}\rho U_{av}^2 \tag{4}$$

is shown in Fig 8 at axial locations along the test section and for different $\Psi$, $\alpha$ and $Re$. It can be seen that $C_{p_o}$ increases with decreasing $Re$ and increasing $\alpha$ and $\Psi$, in agreement with the results of Brighton and Jones[8] who considered only $\Psi = 0$ in fully developed flow.

If an order of magnitude analysis is applied to the momentum equation in the radial direction it is found that:

$$\frac{\partial C_p}{\partial R} \approx \frac{W^2}{R} \tag{5}$$

and so numerical integration from $R = 1$, where $C_p = C_{p_o}$, to $R = \alpha$ yields the pressure coefficient at the inner wall since $W$ is known. There is no doubt that such a procedure would incur inaccuracies but in any even the pressure gradient can be used to describe the flow behaviour. Fig 9 shows the variation of $\partial C_p / \partial R$ over the $\alpha = 0.51$ annulus for $\Psi = 15°$ and 45°. Naturally, the variation of $W$ is accentuated and again it is found, by detailed examination of the curves, that the core region, ie between the location of the peak and $R = 0.9$, displays a free vortex behaviour since the pressure gradient varies as $R^{-3}$. Near the inner wall $\partial C_p / \partial R$ is approximately linear indicating a near forced vortex flow.

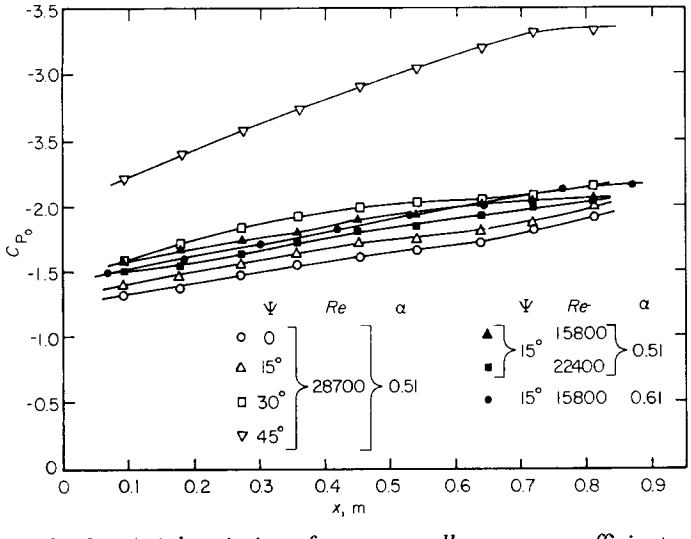


*Fig 8 Axial variation of concave wall pressure coefficient*

## Conclusions

Boundary layer suction applied to the inner and outer walls of the annulus ahead of the test section has been used to investigate swirling flows without the complexity of an undefined shear flow at entry. The development of the flow over the first fifteen hydraulic diameters displays a number of complicated features which require further detailed study before a complete description can be given. There are, however, indications that several phases with distinctive properties exist before a final, fully-developed phase is reached in which the radial distribution of the mean axial velocity remains unchanged with increase in axial distance downstream.

A number of details are readily observable. At the inlet there is a rapid change from a potential flow velocity distribution to one in which a shear flow exists close to each wall of the annulus and a substantially free-vortex at the core. As distance increases downstream the wall boundary layers grow in thickness and the location of maximum tangential velocity moves progressively away from the inner wall. Generally, the radial velocity component is small and the axial velocity component is weakly dependent on swirl. The results shown indicate that the axial rate of decay of swirl, represented by a swirl parameter, increases with inlet swirl, radius ratio and decreasing Reynolds number. The gauge pressure on the outer wall of the annulus, represented by a pressure coefficient, is negative and decreases along the wall from inlet to outlet. No measurements of pressure could be taken on the inner wall. However, an order of magnitude analysis applied to the equations of motion shows that the radial pressure gradient is always positive and so it may be implied that the pressure on the inner wall is less than that on the outer wall.

## References

1. **King M. K., Rothfus R. R. and Kermode R. I.** Static pressure and velocity profiles in swirling incompressible tube flow, *J.A.I.Ch.E., 1969*, **15**(6), *837–842*

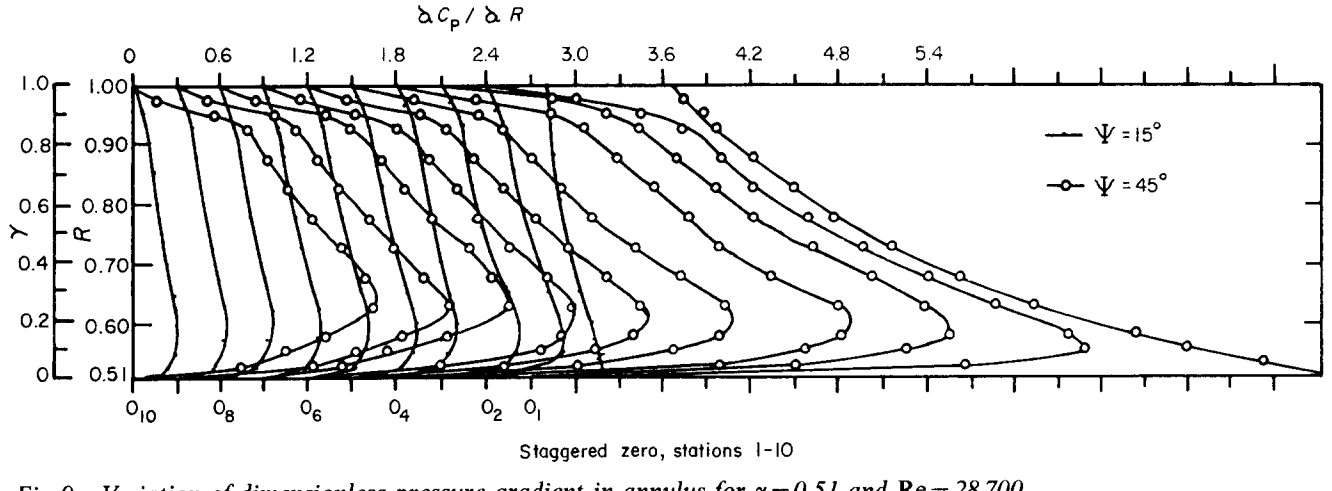


*Fig 9 Variation of dimensionless pressure gradient in annulus for $\alpha = 0.51$ and* Re $= 28\,700$

2. **Wolf J. R., Lavan Z. and Fejer A. A.** Measurements of the decay of swirl in turbulent flow. *AIAAJ, 1969*, **7**, *971–973*

3. **Backshall R. G.** The boundary layer velocity distribution in turbulent swirling pipe flow. *J. Basic Engng., Trans. ASME, 1969*, **91**, *729–733*

4 **Senoo Y. and Negata T.** Swirl flow in long pipes with different roughness. *Bull. JSME, 1972*, **15**(*90*), *1514–1521*

5. **Yajnik K. S. and Subbaiah M. V.** Experiments on the swirling turbulent flows. *J. Fluid Mech., 1973*, **60**(*4*), *665–687*

6. **Murakami M., Kito O., Katayama Y. and Iida Y.** An experimental study of swirling flow in pipes. *Bull. JSME, 1976*, **19**(*128*), *118–126*

7. **Yeh H.** Boundary layer along annular walls in a swirling flow. *Trans. ASME, 1958*, **80**, *767–776*

8. **Brighton J. A. and Jones J. B.** Fully developed turbulent flow in annuli. *J. Basic Engng, Trans. ASME, 1964*, **86**, *835–844*

9. **Okiishi T. H. and Serovy G. K.** An experimental study of the turbulent flow boundary layer development in smooth annuli. *J. Basic Engng, Trans. ASME, 1967*, **89**, *823–836*

10. **Quarmby A.** An experimental study of turbulent flow through concentric annuli. *Intl. J. Mech. Eng. Sci., 1967*, **9**, *205–221*

11. **Gutstein M. U., Convers G. L. and Peterson R.** Theoretical analysis and measurement of single phase pressure losses and heat transfer for helical flow in a tube. *NASA Tech. Note, D-6097, 1970*

12. **Scott C. J. and Rask D. R.** Turbulent viscosity for swirling flow in a stationary annulus. *J. Fluid Engng., Trans ASME, 1973*, **95**, *557–566*

13. **Clayton B. R. and Morsi Y. S. M.** Determination of principal characteristics of turbulent swirling flow along annuli – Part 2: Measurement of turbulence components. *Intl J. Heat and Fluid Flow, to be published (March 1985)*

14. **Morsi Y. S. M.** Analysis of turbulent swirling flows in axisymmetric annuli. *PhD Thesis, University of London, 1983*

15. **Tuckey P. R., Morsi Y. S. M. and Clayton B. R.** Experimental analysis of three dimensional flow fields. *Intl J. Mech. Engng Educ., 1984*, **12**, *149–166*

16. **Clayton B. R. and Morsi Y. S. M.** Theoretical analysis of turbulent swirling flow along axisymmetric annuli. *In preparation*

# BOOK REVIEW

## Heat and Mass Transfer in Rotating Machinery

Eds D. E. Metzger and N. H. Afgan

During the last two decades heat transfer problem solving has become increasingly important to the design of gas turbine aero-engines. These engines are characterised by their high power concentration and low specific fuel consumption, leading to low weight, small size, high thrust-to-weight ratio and low operational fuel consumption. In civil engines fuel consumption is of paramount importance, such that today's advanced technology high bypass ratio engines result in about 40% less fuel per passenger seat being consumed than was the case ten or more years ago. There are two major factors contributing to these achievements: high compression ratio and turbine entry temperature giving high thermal efficiency and power density. As a consequence the heat transfer engineer has become much more important in the design of aero-engines and research efforts into heat transfer and associated mass transfer problems have intensified.

The International Centre for Heat and Mass Transfer in Belgrade, Yugoslavia, organised a symposium in September 1982, of which this book is the proceedings. Metzger was Chairman of the Symposium Committee and Afgan is the Scientific Secretary to ICHMT. The general format of the book is much the same as the symposium in which the papers have been organised into the generic research areas; rotating tubes and channels (6 papers), rotating surfaces and enclosures (11 papers), experimental techniques (8 papers), gas turbines (10 papers), steam turbines (6 papers) and rotating heat pipes and thermosyphons (6 papers). The contents of the papers are of excellent quality and cover in depth major areas of interest in the transfer of heat and mass in rotating machinery.

Conclusions to be drawn from the book are that whereas it has been traditional for the heat transfer engineer to concentrate his activities on the cooling of 'hot parts', notably the combustor and turbine, he now has responsibilities for the thermal behaviour of all other parts, including the 'cold parts' such as the fan, compressor, labyrinth seals, bearings, etc. The heat transfer tasks involved in major engine components are such that nearly all aspects of heat transfer technology are met in aero-engines, and this is clear from the contents of the papers presented and the generic format of the book. Detailed models of heat transfer processes still remain to be developed and many phenomena are not fully understood, so continued research of the kind described in the book is called for.

The book covers many aspects of design development and research in rotating machinery. It is a timely and valuable addition to the engine designer and heat and mass transfer research worker.

A. Brown
Royal Military College of Science,
Shrivenham, Wiltshire, UK

Published, price DM 198 or $73.90 (approx.), by Hemisphere/Springer-Verlag. Hemisphere Publishing Corporation, Berkeley Building, 19W 44th Street, New York, NY 10036, USA, or Springer-Verlag, Heidelberger Platz 3, Postfach, D-1000 Berlin 33, FRG